

Article

Hydrogen-Cycling during Solventogenesis in *Clostridium acetobutylicum* American Type Culture Collection (ATCC) 824 Requires the [NiFe]-Hydrogenase for Energy Conservation

Katherine L. Germane ^{1,*}, Sanchao Liu ¹, Elliot S. Gerlach ¹, Alice M. Savage ²,
Rebecca L. Renberg ³ , Theresah N. K. Zu ¹ , Hong Dong ², Scott D. Walck ⁴,
Matthew D. Servinsky ¹ and Christian J. Sund ^{1,*}

¹ US Army Research Laboratory, RDRL-SEE-B, 2800 Powder Mill Road, Adelphi, MD 20783, USA; Sanchao.Liu.civ@mail.mil (S.L.); Elliot.S.Gerlach.civ@mail.mil (E.S.G.); Theresah.Zu.civ@mail.mil (T.N.K.Z.); Matthew.D.Servinsky@mail.mil (M.D.S.)

² US Army Research Laboratory, Aberdeen Proving Ground, MD 21005, USA; Alice.M.Savage2.civ@mail.mil (A.M.S.); Hong.Dong.civ@mail.mil (H.D.)

³ General Technical Services, 1451 Route 34 South, Suite 301, Wall Township, NJ 07727, USA; Rebecca.L.Renberg.ctr@mail.mil

⁴ Survice Engineering, 4695 Millennium Drive, Belcamp, MD 21017, USA; Scott.d.walck2.ctr@mail.mil

* Correspondence: Katherine.Germane.civ@mail.mil (K.L.G.); Christian.J.Sund.civ@mail.mil (C.J.S.); Tel.: +1-3013940604 (K.L.G.); +1-3013941880 (C.J.S.)

Received: 20 June 2018; Accepted: 17 July 2018; Published: 19 July 2018



Abstract: *Clostridium acetobutylicum* has traditionally been used for production of acetone, butanol, and ethanol (ABE). Butanol is a commodity chemical due in part to its suitability as a biofuel; however, the current yield of this product from biological systems is not economically feasible as an alternative fuel source. Understanding solvent phase physiology, solvent tolerance, and their genetic underpinning is key for future strain optimization of the bacterium. This study shows the importance of a [NiFe]-hydrogenase in solvent phase physiology. *C. acetobutylicum* genes *ca_c0810* and *ca_c0811*, annotated as a HypF and HypD maturation factor, were found to be required for [NiFe]-hydrogenase activity. They were shown to be part of a polycistronic operon with other *hyp* genes. Hydrogenase activity assays of the $\Delta hypF/hypD$ mutant showed an almost complete inactivation of the [NiFe]-hydrogenase. Metabolic studies comparing $\Delta hypF/hypD$ and wild type (WT) strains in planktonic and sessile conditions indicated the hydrogenase was important for solvent phase metabolism. For the mutant, reabsorption of acetate and butyrate was inhibited during solventogenesis in planktonic cultures, and less ABE was produced. During sessile growth, the $\Delta hypF/hypD$ mutant had higher initial acetone: butanol ratios, which is consistent with the inability to obtain reduced cofactors via H₂ uptake. In sessile conditions, the $\Delta hypF/hypD$ mutant was inhibited in early solventogenesis, but it appeared to remodel its metabolism and produced mainly butanol in late solventogenesis without the uptake of acids. Energy filtered transmission electron microscopy (EFTEM) mapped Pd(II) reduction via [NiFe]-hydrogenase induced H₂ oxidation at the extracellular side of the membrane on WT cells. A decrease of Pd(0) deposits on $\Delta hypF/hypD$ comparatively to WT indicates that the [NiFe]-hydrogenase contributed to the Pd(II) reduction. Calculations of reaction potentials during acidogenesis and solventogenesis predict the [NiFe]-hydrogenase can couple NAD⁺ reduction with membrane transport of electrons. Extracellular oxidation of H₂ combined with the potential for electron transport across the membrane indicate that the [NiFe]-hydrogenase contributes to proton motive force maintenance via hydrogen cycling.

Keywords: [NiFe]-hydrogenase; *Clostridium acetobutylicum*; butanol; acetone; ethanol; solventogenesis; sessile; planktonic; hydrogen uptake

1. Introduction

Solventogenic *Clostridia* have been used to produce the commodity chemicals acetone, butanol, and ethanol from renewable feedstocks via the acetone, butanol, and ethanol (ABE) fermentation process [1,2]. The model solventogenic organism is *Clostridium acetobutylicum*, which ferments a variety of carbohydrates that is prevalent in biomass [3]. In batch culture, the organism's metabolism proceeds from an initial acidogenic phase, producing mostly acetate and butyrate, to a solventogenic phase, where acetate and butyrate are reabsorbed, and along with a carbohydrate, are converted to acetone, butanol, and ethanol [1]. The redox state of the organism is important for the relative distribution of acids and solvents produced [4]. Hence, there have been numerous demonstrations of altering metabolic output by manipulation of electron flow via metabolic inhibitors, feedstock selection, and genetic engineering [4–7].

An important mechanism for maintaining redox balance in *C. acetobutylicum* is the production of H₂ [8]. Electron flow through H₂ in *Clostridium spp.* is primarily controlled by two types of hydrogenases: H₂-evolving hydrogenases and H₂-uptake/respiratory hydrogenases [9]. [FeFe]-hydrogenases are responsible for the production of H₂, whereas [NiFe]-hydrogenases are involved in H₂ oxidation and possibly the production of NADH/NAD(P)H [9].

Internal production of H₂ by the [FeFe]-hydrogenase increases intracellular pH (via proton reduction) and it provides oxidized ferredoxin for central metabolism [8,10]. Oxidized ferredoxin is required for the major pyruvate decarboxylating enzyme, pyruvate ferredoxin oxidoreductase (PFOR), and the butyryl-CoA dehydrogenase (BCD), which is essential for butyrate and butanol production [1,11]. There are two HydA [FeFe]-hydrogenase genes in *C. acetobutylicum*: HydA1, which is constitutively expressed, and HydA2, which is induced during solventogenesis [10,12]. While the HydA1 operates primarily in the direction of H₂ production during batch fermentations, the enzyme reaction is reversible and it is important for the H₂ dependent reduction of nitroaromatic compounds [5,10].

The [NiFe]-hydrogenase is the lesser studied hydrogenase of *Clostridia*, pervasive among the different species, and is believed to be involved in H₂ uptake [9]. An siRNA knock down of the [NiFe]-hydrogenase in *C. saccharoperbutylacetonicum* N1, to our knowledge the only published study of *Clostridial* [NiFe]-hydrogenase activity, showed a marked decrease in butanol production, thereby indicating physiological evidence of hydrogen uptake [13]. A bioinformatics analysis of *Clostridial* hydrogenases indicates that *C. acetobutylicum* ATCC 824 encodes probable a group 1 [NiFe]-hydrogenase, and the maturation factors genes are located on both the chromosome and pSol megaplasmid [9]. The predicted protein sequences are similar to the *C. saccharoperbutylacetonicum* N1 [NiFe]-hydrogenase, and previous studies have shown *C. acetobutylicum* mRNA expression from the corresponding genes is induced during solventogenesis [12]. Increased expression during solvent phase suggests the *C. acetobutylicum* [NiFe]-hydrogenase is important for solventogenic growth phase, but its exact role is not understood.

In this report, we begin to elucidate the function of *C. acetobutylicum*'s [NiFe]-hydrogenase and associated maturation factors. Interruption of the [NiFe]-hydrogenase maturation factor *hypF* homolog gene *ca_c0810*, and the subsequent gene in the operon, *hypD* homolog *ca_c0811*, inhibited hydrogenase activity, thereby indicating their role in maturation. The *hypF/hypD* mutant displayed altered metabolism, as consistent with a defect in hydrogen uptake, resulting in decreased ABE output and altered product ratios in early solventogenesis. Palladium nanoparticle formation at the site of hydrogen gas oxidation identified that the [NiFe]-hydrogenase is membrane localized with the catalytic subunit facing the extracellular side of the membrane. Calculated net reduced cofactor production

over time for WT and mutant strains indicate a role in NADH production for the [NiFe]-hydrogenase during solventogenesis. Together with energetic calculations and sequence analysis, the results indicate the [NiFe]-hydrogenase likely couples H₂ oxidation with electron transport and intracellular NAD⁺ reduction, thereby acting as a crude proton pump that conserves energy via hydrogen cycling.

2. Materials and Methods

2.1. Bacterial Strain Propagation

Clostridium acetobutylicum ATCC 824 (Wild type, or WT) was obtained from American Type Culture Collection (ATCC), and *Clostridium acetobutylicum* M5 (M5), which lacks the pSol megaplasmid, was provided by the Papoutsakis laboratory [14]. Wild type and derivative strains were maintained as anaerobic spore suspensions at room temperature in potato glucose medium (PGM) containing: 150.0 g·L⁻¹ potato (grated), 10.0 g·L⁻¹ glucose, 0.5 g·L⁻¹ (NH₄)₂SO₄, and 3.0 g·L⁻¹ CaCO₃ [15]. The media was boiled for one hour, strained, and then autoclaved. M5 was maintained under anaerobic conditions on *Clostridial* growth medium (CGM) agarose plates, as previously described [6, 16]. *C. acetobutylicum* strains were propagated in CGM or P2 medium containing 6.0% glucose, as previously described [12]. Cultures were grown in a Coy anaerobic chamber (Coy Lab Products) at 37 °C in an atmosphere of 5.0% H₂, 5.0% CO₂, and 90.0% N₂.

2.2. Construction of HypF/HypD Mutant

The *hypF* annotated gene, *ca_c0810*, was disrupted using a group II intron based system (ClosTron) [17]. An intron insertion site was predicted at 153|154s in the sense sequence using the TargeTron Gene Knockout System website (MilliporeSigma, St. Louis, MO, USA) [18]. The target insert was designed using the intron prediction primers, obtained from Biobasic, and cloned into pMTL007C-E2 (Table S2) (GenBank accession no. HQ263410.1) [19]. pMTL007C-E2: *CachypF* was transformed into WT *C. acetobutylicum* ATCC 824, mutants were screened as previously described, and then confirmed via PCR and southern blot [20,21] (see Table S1 and Figure S1). One mutant was verified to have integration in *ca_c0810* and was designated CacATCC824-*hypF:CT*(Δ *hypF/hypD*).

2.3. Construction of Complement Strains

The *ca_c0810/ca_c0811* complement plasmid was designed using the phosphotransbutyrylase promoter (ptb) sequence followed by the full *ca_c0810/ca_c0811* genetic sequence, position 935667 to 939040 on the WT *C. acetobutylicum* ATCC 824 genome, and was synthesized by Biobasic (Genbank accession nos. NP_347446 and NC_003030.1). The sequence was cloned into the *AscI/SbfI* sites of pMTL007C-E2, retaining the *repH*, *catP*, *ColEI*, and *traJ* elements and designated pMTL007C-E2: *PtbhypFhypD*. pMTL007C-E2: *PtbhypFhypD* was transformed into the Δ *hypF/hypD* strain and control complement strains were created by the addition of an empty pMTL007C-E2 plasmid into Δ *hypF/hypD* and WT *C. acetobutylicum* ATCC 824, as previously described [21]. The complement strains were designated CacATCC824-*hypF:PtbhypFhypD* (Δ *hypF/hypD:p-hypF/hypD*), CacATCC824-*hypF:pMTL*(Δ *hypF/hypD:pMTL*), and CacATCC824-*pMTL*(WT:pMTL).

2.4. Sample Collection for RNA Seq Data

Static planktonic cultures were grown in P2 medium containing 6.0% glucose, as previously described [12]. Twenty milliliters of overnight cultures of WT *C. acetobutylicum* and Δ *hypF/hypD* were grown to OD₆₀₀ of 0.8. Two milliliters of the overnight culture was then sub-cultured in triplicate to glass bottles containing 60.00 mL glucoseP2 medium. Two milliliters samples of planktonic cultures were collected at 24 h post sub-culture, which is the time point Liu et al. described to have the highest expression level of the genes of interest [12]. Samples were treated with a final concentration of 30 µg·mL⁻¹ rifampicin, incubated for 10 min on ice, and then treated with RNA protect (Qiagen, Hilden, Germany), as previously described [16].

2.5. RNA Extraction, Purification, and rRNA Depletion

Total RNA was isolated using the miRNeasy Mini Kit (Qiagen, Hilden, Germany), according to the manufacturer's protocol, with an additional homogenization and mechanical disruption step using a bead beater (BioSpec, Bartlesville, OK, USA) with Zirconia/Silica beads (BioSpec). RNA quality was assessed using the 2100 BioAnalyzer (Agilent Technologies, Santa Clara, CA, USA), quantified with a Qubit fluorimeter (Thermo Fisher Scientific, Waltham, MA, USA), and then stored at $-80\text{ }^{\circ}\text{C}$ prior to DNase treatment. DNA was removed using the TURBO DNA-free kit (Thermo Fisher Scientific), according to the manufacturer's protocol. RNA was again quantified and quality assessed, as stated above. Ribosomal RNA was removed using the Ribo-Zero rRNA Removal Kit for Gram-Positive Bacteria (Illumina, San Diego, CA, USA), according to the manufacturer's protocol. The quality of rRNA depleted samples was assessed once more prior to processing for sequencing library generation.

2.6. Sequencing Library Preparation

TruSeq Stranded mRNA Sample Preparation Kit (Illumina) was used to prepare the rRNA depleted RNA for sequencing, according to the manufacturer's protocol. Libraries were quantified using the Kapa Library Quantification Kit (KapaBiosystems, Wilmington, MA, USA), according to the manufacturer's instructions, then normalized and pooled for sequencing, according to the Denature and Dilute Libraries Guide for the NextSeq 500 (Illumina, San Diego, CA, USA). Pooled libraries were paired end sequenced on a NextSeq 500 (Illumina, San Diego, CA, USA).

2.7. RNA-Seq Data Analysis

Samples had an average of 20 million reads each, were assessed for quality using FastQC, and then trimmed to remove Illumina adaptors and low quality bases using Trimmomatic [22]. Operon structure predictions were performed using Rockhopper [23].

2.8. Hydrogenase Zymogram

Hydrogenase assay steps were performed under anaerobic conditions. Five milliliters cultures of $\Delta hypF/hypD$, WT, M5, and $\Delta hypF/hypD:P-hypF/hypD$ were grown in CGM containing 6.0% glucose at $37\text{ }^{\circ}\text{C}$ to an OD_{600} of 1.2. Cells were isolated via centrifugation (6000 rpm for 10 min in a Corning LSE centrifuge) and the resulting pellets were subsequently washed twice with 10 mL of PBS (MilliporeSigma, St. Louis, MO, USA), isolating cells between washes by centrifugation, as above. The pellets were then suspended in 800 μL CellLytic™ B Plus (MilliporeSigma, St. Louis, MO, USA), 1.0% dodecyl maltoside, and benzonase, and then subjected to 10 consecutive 15 s intervals of sonication on ice. The lysates were subjected to non-denaturing PAGE on Mini-PROTEAN® TGX™ gels (Bio-Rad Laboratories Inc., Hercules, CA, USA). Hydrogenase activity was visualized by incubation of gel in 50.0 mM MOPs buffer (pH 8.0), 1.0 mM benzyl viologen (BV), and 2.0 mM 2,3,5-triphenyltetrazolium chloride (TTC), as previously described by Pinske et al. [24].

2.9. Growth and Metabolite Studies

Agitated and static planktonic culture studies were performed in CGM containing 5% glucose and grown in DasGip (Eppendorf, Hamburg, Germany) bioreactors (Eppendorf) for 48 h. Two hundred milliliters overnight cultures of WT and $\Delta hypF/hypD$ were grown to OD_{600} of 0.8 in CGM containing 5.0% glucose under anaerobic conditions. Thirty milliliters were then sub-cultured into 1 L of CGM containing 5.0% glucose in DasGip (Eppendorf, Hamburg, Germany) bioreactors under anaerobic conditions with Rushton impellers running at either 400 rpm or 0 rpm, in duplicate. The headspace of the bioreactors were flushed with N_2 . Samples for metabolite analysis were taken every 24 h. The samples were clarified via filtration through a 0.2 μm PES syringe filter (Corning, NY, USA) and stored at $-20\text{ }^{\circ}\text{C}$.

Sessile culture studies were performed in comparison to static planktonic cultures in P2 medium containing 6.0% glucose in glass bottles, as previously described [12]. Twenty milliliters overnight cultures of WT and $\Delta hypF/hypD$ were grown to OD₆₀₀ of 0.8. Two milliliters were then sub-cultured into glass bottles under anaerobic conditions (without N₂ headspace flushing) containing 60.0 mL P2 medium, with either 2 g of autoclaved cotton balls for sessile studies, or without cotton balls for static planktonic culture studies, both in triplicate. The complement strains, $\Delta hypF/hypD:p-hypF/hypD$, $\Delta hypF/hypD:pMTL$, and WT:pMTL were grown overnight in similar conditions, except the overnight cultures contained final concentrations of 30 $\mu\text{g}\cdot\text{mL}^{-1}$ chloramphenicol for all strains and 40 $\mu\text{g}\cdot\text{mL}^{-1}$ for the $\Delta hypF/hypD:p-hypF/hypD$ and $\Delta hypF/hypD:pMTL$ strains. Two milliliters of the overnight complement strains were then sub-cultured into glass bottles under anaerobic conditions (without N₂ headspace flushing) containing 60.0 mL P2 medium and a final concentration of 30 $\mu\text{g}\cdot\text{mL}^{-1}$ chloramphenicol, with either 2 g of autoclaved cotton balls for sessile studies, or without cotton balls for static planktonic culture studies, all in triplicate. The cultures were spiked with a final concentration of 30 $\mu\text{g}\cdot\text{mL}^{-1}$ of chloramphenicol every 48 h to maintain the plasmids. Samples for metabolite analysis were taken every 24 h for 144 h. Metabolite samples were clarified via filtration through a 0.2 μm PES syringe filter (Corning) and then stored at $-20\text{ }^{\circ}\text{C}$. HPLC analysis of samples for metabolite concentrations was performed on an Agilent 1200, as previously described [6,25]. Samples were injected into the HPLC system, eluted isocratically, and quantified using an external calibration curve of pure known components as standards.

2.10. Reduction of Palladium

To determine location of the NiFe hydrogenases, 20 mL WT *C. acetobutylicum* ATCC 824, heat killed (1 h at $80\text{ }^{\circ}\text{C}$) WT *C. acetobutylicum* ATCC 824, pSol null *C. acetobutylicum* M5, and [NiFe]-hydrogenase mutant *C. acetobutylicum* $\Delta 810/811$ grown to OD₆₀₀ of 1.5 in 6.0% glucose CGM were centrifuged for 15 min at 6000 RPM (Corning LSE centrifuge) in anaerobic conditions, and then the supernatant was removed. The pellets were washed twice with 20 mL of 20 mM MOPS buffer (pH 7.2) and re-suspended with 20 mL of the same buffer. The resting cells were sparged with oxygen free nitrogen (OFN) for 10 min. Two millimolar Pd(II) solution was made by dissolving sodium tetrachloropalladate (Na₂PdCl₄) in 0.01 M HNO₃, pH 2.3 [26]. The Pd(II) solution was degassed for 10 min, then flushed with OFN for 10 min. The Pd(II) solution was added to the suspension of resting cells to give a mass ratio of 1:4 Pd(II): dry biomass. The mixture was incubated for 30 min at $37\text{ }^{\circ}\text{C}$, with occasional shaking to allow for initial absorption of Pd(II). Pd(II) reduction was initiated by flushing the mixture with H₂ gas for 2 h at $37\text{ }^{\circ}\text{C}$.

2.11. Sample Preparation for TEM

The Pd loaded bacteria were rinsed twice with 20 mL distilled water, fixed in 1 mL of 2.5% (*w/v*) glutaraldehyde for 30 min, centrifuged, resuspended in 0.5 mL 0.1 M phosphate buffer (pH 7), and stained in a final concentration of 1% osmium tetroxide in 0.1 M phosphate buffer (pH 7) for 60 min. The bacteria after staining were centrifuged and the pellets were freeze-dried. The dried bacterial samples were embedded in epoxy resin (low viscosity embedding kit) (Electron Microscopy Sciences, Hatfield, PA, USA) and cured overnight at $60\text{ }^{\circ}\text{C}$ in the oven. Samples for TEM were prepared using a Leica EM UC7 ultramicrotome with a Diatome 35° wet diamond knife (Leica Microsystems, Buffalo Grove, IL, USA). Sections were cut from the embedded samples at room temperature to a thickness of approximately 200 nm. Sections were then coated with a 2 nm carbon film using a Leica Microsystems EM ACE600 high vacuum sputter coater equipped with a carbon thread coater (Leica Microsystems, Buffalo Grove, IL, USA).

2.12. TEM Imaging of Samples

The scanning transmission electron microscopy (STEM) mode of a JEOL JEM-2100F TEM (JEOL USA Inc., Peabody, MA, USA) equipped with a Gatan 806 high-angle annular dark field (HAADF)

detector (Gatan, Pleasanton, CA, USA) was used to collect STEM-HAADF images from each sample. The microscope was operated at 200 kV, with a spot size of 0.2 nm, and a 40 μm condenser aperture that gave a convergence angle of 8.3 mrad. The STEM-HAADF collection angle range was 48–148 mrad. Gatan Microscopy Suite version 1.85 with DigiScan was used to collect the images.

2.13. Energy Filtered TEM

Energy Filtered TEM (EFTEM) jump ratio and elemental map images were acquired from C-K, O-K, and Pd-L edges using Gatan's suggested energy windows. For each filtered image, ten images were acquired at a hardware binned value of 8 to give 256×256 pixel images at an exposure that minimized drift effects. Individual image exposures were typically 5 s.

2.14. Reduction Potential Calculations

Total reaction potentials for a range of external pH values were calculated by summing the potentials of individual oxidoreduction reactions and electron transport across the membrane. All of the calculations assumed standard conditions and an H_2 concentration of 1 bar. Previously determined pH-dependent membrane potentials, proton motive force (pmf), and intracellular vs. extracellular pH values were utilized [27]. Reduction potentials for NAD^+/NADH and $\text{NADP}^+/\text{NADPH}$ were calculated for solvent phase cells using the Nernst equation and intracellular concentrations reported by Amador-Noguez et al. [28]. Electron transport values were obtained using the previously reported membrane potentials and assumed transport of two electrons [27]. Additional details of the calculations are available in the supplemental material Figure S4.

3. Results

3.1. [NiFe]-Hydrogenase Operon Structure

The operon structures of the [NiFe]-hydrogenase and putative maturation factor genes, as shown in Figure 1, were determined by DOOR² predictions and Rockhopper analysis of RNA-Seq data (Figure S1), Data available upon request) [23,29–31]. The analysis indicated that the chromosomally based genes *ca_c0808* through *ca_c0811* were transcribed as a single operon (Figure 1), which is inconsistent with MetaCyc predictions where *ca_c0808* was predicted to be in a separate operon [23,30,32]. The pSol located genes *ca_p0141* through *ca_p0146* were also part of a single operon (Figure 1) [23,29,30]. The putative functions of *ca_p0144* and *ca_p0146* are unknown, but a BLASTP analysis of the *ca_p0144* derived amino acid sequence indicated that it contains a putative heme binding domain, which could bind a cofactor that is involved in electron transfer from the hydrogenase to other redox enzymes that are similar to other organisms [9,33–35]. A BLASTP analysis of the *ca_p0146*-derived amino acid sequence indicates that it is similar to HypF, but the amino acid sequence does not contain the conserved zinc binding motif found in other HypF proteins, suggesting *ca_p0146* is a truncated HypF1-like protein, which has been found in other organism, such as *Ralstonia eutrophia* [36,37]. While HypF1 seems to be functional in *R. eutrophia*, the purpose of two HypF paralogs in *C. acetobutylicum* is not known.

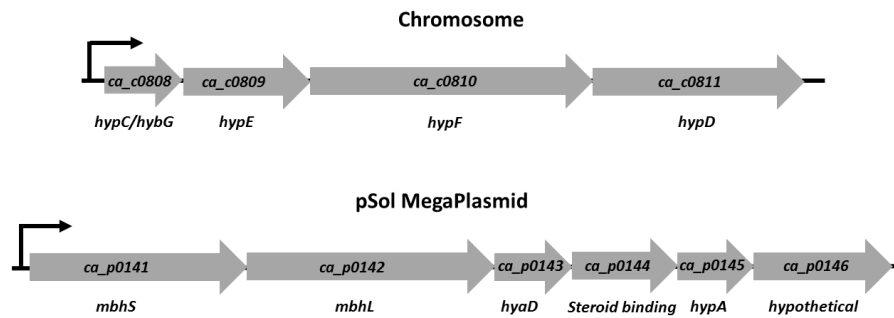


Figure 1. Genetic maps of [NiFe]-hydrogenase subunit and maturation factor operons. Black arrows denote transcriptional start sites for operons indicated by DOOR² and Rockhopper using RNA-Seq data (Figure S2) [22,28]. One operon is located on the chromosome and includes genes for maturation factors HypC/HybG, HypE, HypF, and HypD; annotated *ca_c0808*, *ca_c0809*, *ca_c0810*, and *ca_c0811*, respectively. The second operon is located on the pSol megaplasmid, and it includes genes for the two hydrogenase subunits, the HyaD protease, a putative heme binding protein, possible HypA maturation factor, and a hypothetical truncated HypF like protein; annotated *ca_p0141*, *ca_p0142*, *ca_p0143*, *ca_p0144*, *ca_p0145*, and *ca_p0146*, respectively.

3.2. Disruption of [NiFe]-Hydrogenase Maturation

Preceding studies have shown [NiFe]-hydrogenase activity inhibition through partial disruption by siRNA in *C. saccharoperbutylacetonicum* [13]. In the current study, [NiFe]-hydrogenase activity in *C. acetobutylicum* was knocked out by interruption of the maturation factor *hypF* gene, *ca_c0810*, through the use of the ClosTron type II intron, which also interrupted transcription of *hypD* (*ca_c0811*) (Figure S2). Analysis of hydrogenase activities with zymograms, Figure 2, showed a reduction of hydrogenase activity in the $\Delta hypF/hypD$ mutant when compared to WT. The activity profile was similar to the [NiFe]-hydrogenase null *C. acetobutylicum* M5 strain, which lacks the pSol plasmid containing the *ca_p0141-0146* operon, indicating that the lowered hydrogenase activity is due to the loss of active [NiFe]-hydrogenase [24]. The [NiFe]-hydrogenase activity was recovered by complementation of the $\Delta hypF/hypD$ mutant with a plasmid containing the *ca_c0810* and *ca_c0811* genes expressed using the phosphotransbutyrylase promoter ($\Delta hypF/hypD:p-hypF/hypD$). Residual hydrogenase activity in both the M5 and mutant strain is likely due to activity of the [FeFe]-hydrogenases.

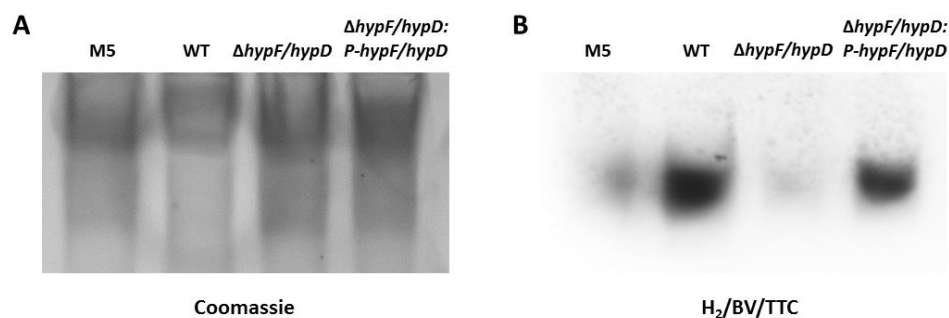


Figure 2. Zymogram of hydrogenase activity showing HypF/HypD is required for H₂ dependent reduction of 2.0 mM 2,3,5-triphenyltetrazolium chloride (TTC) by the [NiFe]-hydrogenase. Sixty micrograms of total protein derived from M5, WT, $\Delta hypF/hypD$, and $\Delta hypF/hypD:p-hypF/hypD$ grown anaerobically in *Clostridial* growth medium (CGM) containing 6.0% glucose was subjected to non-denaturing PAGE. (A) Image of gel containing cell lysates stained with Coomassie Simply Blue; (B) Image of the gel containing cell lysates stained under a hydrogen atmosphere with benzyl viologen (BV) and TTC as electron acceptors.

3.3. Contribution of [NiFe]-Hydrogenase to Metabolic Output

Previous bioinformatics analysis indicated that the *C. acetobutylicum* [NiFe]-hydrogenase could be used for H₂ uptake [9]. Another study showed increased mRNA levels for the [NiFe]-hydrogenase and maturation factor genes during the solvent phase in sessile and planktonic cells [12]. To determine whether the [NiFe]-hydrogenase is important for solvent phase growth, metabolic outputs of WT and the $\Delta hypF/hypD$ mutant were compared under several growth conditions. The first experiment compared growth in bioreactors on rich medium with agitated and static cultures. Similar to previous experiments, the agitated cultures were expected to have lower dissolved gas (H₂ and CO₂) concentrations when compared to the static cultures [6]. After 24 h of growth in agitated cultures, WT and the $\Delta hypF/hypD$ mutant produced similar quantities of acetate, butyrate, and ethanol. There was slightly more butanol, ~5.7 mM vs. 1.6 mM, in WT cultures when compared to the $\Delta hypF/hypD$ mutant. After 24 h, WT and the $\Delta hypF/hypD$ mutant static bioreactor cultures had produced similar amounts of acetate and butyrate (Table 1). WT produced more ethanol than the $\Delta hypF/hypD$ mutant, ~5.4 mM vs. 2.8 mM, respectively. The largest difference in metabolic output was for butanol; where, after 24 h of growth in the static bioreactors, WT produced ~36.4 mM of butanol as compared to ~5.3 mM produced by the $\Delta hypF/hypD$ mutant.

Table 1. Metabolic output of wild type (WT) and mutant strains in static planktonic (stat.) and agitated (agit.) cultures grown on CGM containing 5.0% glucose in anaerobic bioreactors.

	Glucose Consumed	Acetate	Acetone	Acetoin	Ethanol	Butyrate	Butanol
WT agit.	76.9	28.8	3.4	1.3	1.9	43.7	5.7
$\Delta hypF/hypD$ agit.	63.4	31.5	0.0	0.9	1.9	41.9	1.6
WT stat.	106	24.9	17.9	2.9	5.4	27.2	36.4
$\Delta hypF/hypD$ stat.	63.7	27.6	0.0	1.7	2.8	41.8	5.33
N = 2	Concentrations in mM Time = 24 h						

Further metabolic studies were performed during growth in minimal medium in static planktonic and sessile cultures, since previous studies revealed that these conditions showed an increase in expression of mRNA for the [NiFe]-hydrogenase [12]. Analysis of the $\Delta hypF/hypD$ mutant's metabolic output when compared to WT showed a decrease in total solvent concentrations in planktonic cultures, delayed entry into solventogenesis, and higher acetone to butanol ratios for sessile cultures at 48 h (Figure 3). The decrease in planktonic culture ABE production, from ~14.0 g·L⁻¹ in WT to ~10.6 g·L⁻¹ in the mutant, corresponded to a decrease in sugar utilization in the mutant cultures. Final ABE outputs of sessile cultures were similar between the two strains; however, low ABE concentrations for the mutant, when compared to WT, after 24 h showed there was a delayed entry into solventogenesis by the mutant (Figure 3). $\Delta hypF/hypD$ cultures initially produced higher acetone to butanol ratios than WT in sessile cultures. Between 48 h and 72 h, the metabolism of the $\Delta hypF/hypD$ cultures stalled, as indicated by decreased glucose utilization, and they incurred a metabolic switch, after which glucose consumption and butanol formation resumed. There was a loss in acetone from both cultures in this timeframe, which was likely due to evaporation or stripping. The solvent phase metabolic switch in the sessile $\Delta hypF/hypD$ cultures corresponded to an increase in calculated net NADH produced per mole glucose consumed, and a decrease in net ferredoxin and NADPH production. This was seen in the other cultures when glucose consumption stopped. End point residual concentrations of acetate and butyrate in the $\Delta hypF/hypD$ mutant planktonic cultures, ~25.1 mM and ~17.1 mM, are almost double that of WT planktonic cultures, ~12.5 mM and ~10.1 mM (Figure 3). Additionally, acetate concentrations in the mutant sessile cultures were higher than that of WT sessile cultures, pointing towards an inability of the $\Delta hypF/hypD$ mutant to reabsorb acids during solventogenesis. The shift towards residual oxidized product in the $\Delta hypF/hypD$ mutant, when compared to WT, is consistent with a loss in the ability to uptake hydrogen.

Complementation of WT and the mutant with either an empty pMTL plasmid or a *ca_c0810/ca_c0811* operon and a *ptb* promoter on a plasmid, $\Delta hypF/hypD$:pMTL, WT:pMTL, and $\Delta hypF/hypD$:*p-hypF/hypD*, showed a significant decrease in alcohol formation in planktonic cultures when compared to the non-complemented strains, with $\Delta hypF/hypD$:*p-hypF/hypD* not being able to recover alcohol formation equivalent to WT:pMTL (Figure S3). Alcohol formation in pMTL strains were lower in sessile conditions as well; however, complementation of the mutant strain with the *ca_c0810/ca_c0811* operon recovered alcohol production in sessile conditions. Higher acetone concentrations were not seen in the sessile $\Delta hypF/hypD$ cultures complemented with the empty pMTL, likely due to the presence of the plasmid. High ethanol concentrations in all complement cultures were due to the addition of chloramphenicol dissolved in ethanol for plasmid maintenance.

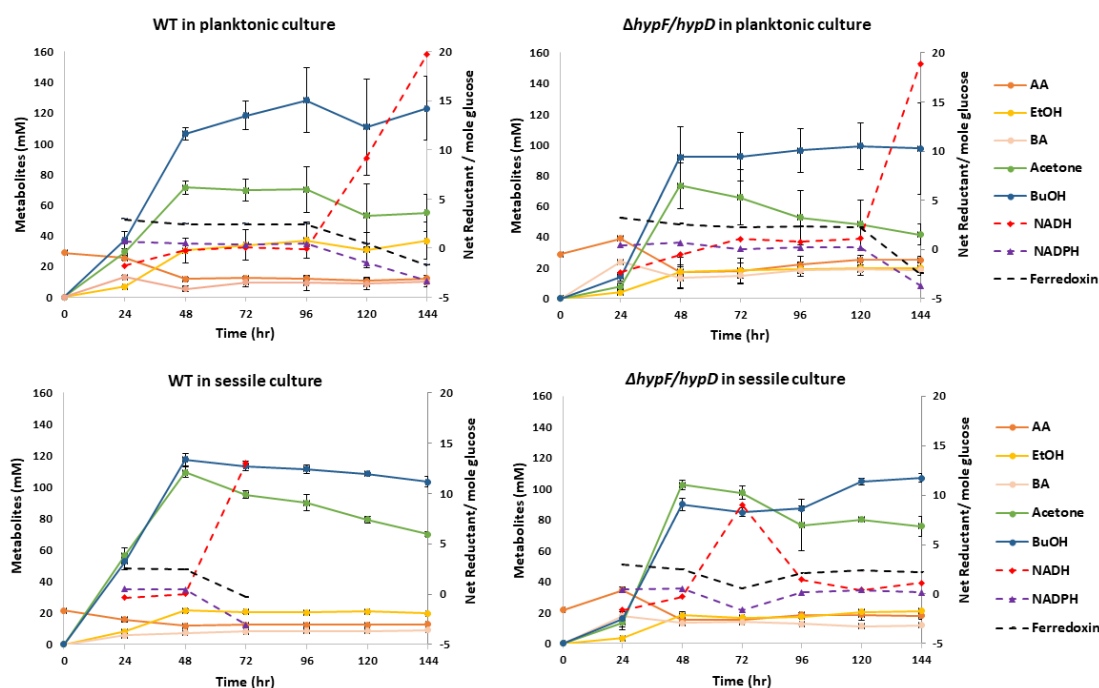


Figure 3. Metabolite profiles of planktonic and sessile cultures grown in minimal medium containing 6.0% glucose from an $N = 3$ experiment. Metabolite concentrations and calculated reduced cofactor formation vs. time for WT and $\Delta hypF/hypD$ cultures. The left Y axes correspond to metabolite concentrations in mM for acetate (AA), ethanol (EtOH), butyrate (BA), acetone, and butanol (BuOH). The right Y axes correspond to calculated reduced cofactors (NADH, NADPH, and ferredoxin) formed from consumption/production of acetyl-CoA calculated from changes in metabolite concentrations from the previous time point. Total calculated reduced cofactors were normalized to glucose utilization for the same time period and expressed as net reductant/mol glucose. These calculations are not included for time points after glucose utilization ceased.

3.4. [NiFe]-Hydrogenase Location

[NiFe]-hydrogenases are classified into groups based on their function, reduction of NAD^+ or $NADP^+$, and location- either soluble membrane associated interior or membrane associated exterior. Although the *C. acetobutylicum* ATCC 824 [NiFe]-hydrogenase is classified as a group 1 [NiFe]-hydrogenase periplasmic enzyme [9], it was not clear how a periplasmic enzyme would play a role in hydrogen cycling based on calculated reduction potentials and whether the classification was correct.

In order to identify the [NiFe]-hydrogenase location, palladium(II) reduction at the catalytic site of the hydrogenase via H_2 gas oxidation was identified based on the formation of palladium nanoparticles. Transmission Electron Microscopy images (TEM) in Figure 4 comparing $\Delta hypF/hypD$,

WT, M5, and dead (heat killed) WT cells showed the formation of palladium nanoparticles at the surface of the cell (Figure 4A–D). EFTEM mapping indicates these particles are on the exterior of the cell, with a decrease in formation nanoparticles in the mutant and the M5 [NiFe]-hydrogenase null strain (Figure 4E,F), demonstrating that the [NiFe]-catalytic subunits are exposed to the extracellular side of the membrane. The presence of some nanoparticles indicate there may be some functional [NiFe]-hydrogenase activity, another redundant protein with the capability to oxidize H₂, or nonspecific reduction of some of the Pd(II) occurring at the membrane.

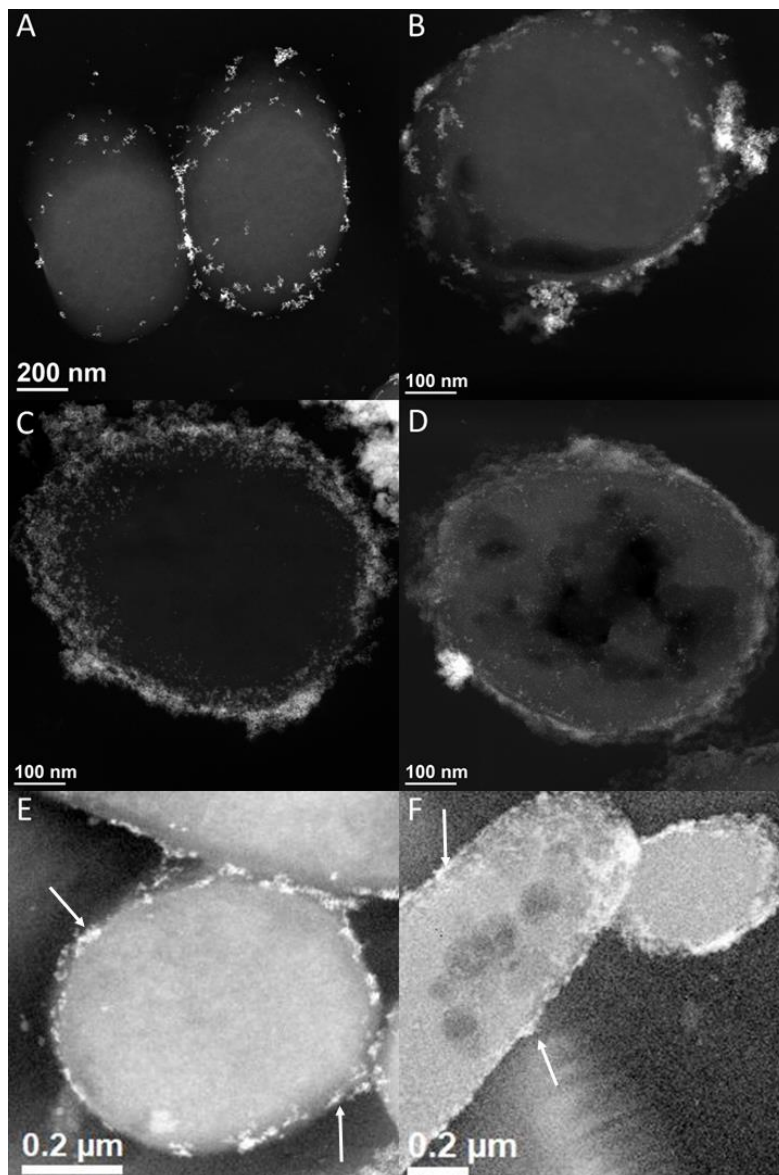


Figure 4. Scanning transmission electron microscopy high-angle annular dark field (STEM-HAADF) dark field images and energy filtered transmission electron microscope (EFTEM) Pd elemental maps comparing Pd(0) nanoparticle formation in different *C. acetobutylicum* strains. STEM-HAADF images of Pd(II)-challenged *C. acetobutylicum* strains with H₂ gas as an electron donor demonstrate localization of Pd(0) nanoparticle formation on the surface of (A) $\Delta hypF/hypD$; (B) M5; (C) WT; and, (D) dead WT cells (heat killed); EFTEM Pd elemental map of (E) $\Delta hypF/hypD$ and (F) WT reveal palladium(0) nanoparticles are located on the extracellular side of the membrane. Palladium(0) maps as bright white particles around the cells. Nanoparticle examples are indicated with white arrows. Scale bars are 200 nm and 100 nm, respectively.

3.5. Possible [NiFe]-Hydrogenase Function

The fate of electrons from hydrogen uptake by *C. acetobutylicum*'s [NiFe]-hydrogenase during solventogenesis is unknown. It is unlikely that ferredoxin is reduced during H₂ uptake. The reduction potential of ferredoxin is too low to accept electrons from H₂ without additional input of energy, since the [FeFe]-hydrogenase (ferredoxin dependent) is likely operating in the direction of H₂ production. Therefore, H₂ uptake by the [NiFe]-hydrogenase is probably coupled to the reduction of a higher potential electron acceptor, such as NAD⁺ or NADP⁺. If the [NiFe]-hydrogenase on the extracellular membrane face oxidizes H₂ and electrons are transported across the membrane to internal electron acceptors, this would lead to energy conservation via H₂ cycling (Figure 5A), similar to sulfate reducing bacteria [38]. To theoretically determine whether external H₂ oxidation could be coupled to internal NAD⁺ or NADP⁺ reduction and the transport of two electrons, the reduction potentials of the reaction at various pHs were calculated, as described in the materials and methods, and the results are shown in Figure 5B. At high pH values, NAD⁺ reduction is not favorable, but at pH 4.5 the reaction potential is slightly above zero, indicating that it is favorable and it would be very responsive to changes in reactant/product concentrations. Values for electron transport coupled to NADP⁺ reduction were well below zero for all of the conditions examined, indicating that the reaction is not favorable.

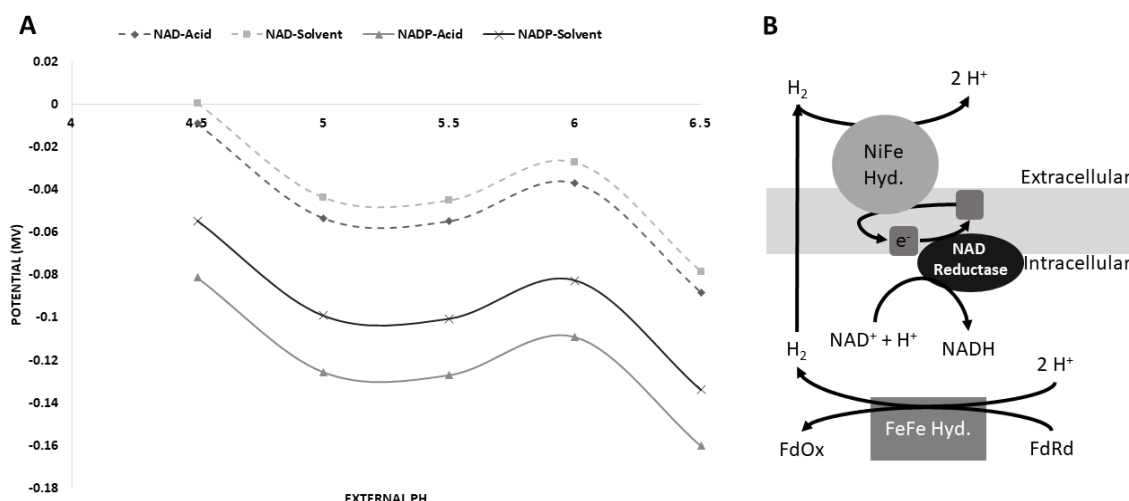


Figure 5. Possible physiological role of [NiFe]-hydrogenase. Panel (A) indicates NAD⁺ and NADP⁺ reduction potentials calculated for the [NiFe]-hydrogenase schematic in panel B for acidogenesis and solventogenesis. Details of the calculations are available in the material and methods and supplemental material; Panel (B) is a schematic of potential hydrogen cycling with the [FeFe]-hydrogenase and [NiFe]-hydrogenase. Protons are reduced to H₂ intracellularly by the [FeFe]-hydrogenase and the H₂ can freely cross the membrane. The [NiFe]-hydrogenase is localized on the extracellular membrane face, converting H₂ to protons externally. Electrons are transported via an electron transport molecule to a cytoplasmic-facing NAD⁺ reductase.

4. Discussion

Control of electron flow is essential to engineer metabolism for the production of desired outputs [39]. Key enzymes for maintaining redox balance are the hydrogenases, which can direct electron flow to proton reduction. Hydrogenases can produce and/or consume H₂, depending on metabolic state and/or the electron carrying cofactors used. In *C. acetobutylicum*, the majority of hydrogenase studies have focused on the [FeFe]-hydrogenases, which are important for ferredoxin recycling and the reduction of xenobiotic compounds [1,5]. The saccharolytic nature of *C. acetobutylicum* and the associated high metabolic flux through PFOR leads to a strong demand for ferredoxin oxidation by the [FeFe]-hydrogenase in growth conditions important for solvent formation [40]. While it has

been demonstrated that the [FeFe]-hydrogenase oxidizes H₂ in vitro, the physiologically relevant need for ferredoxin oxidation indicates that its primary role is H₂ production [10]. During acidogenesis, the H₂/CO₂ ratio is approximately 1.2, but this decreases to ~0.7 during solventogenesis as a result of rerouting the electron flow from H₂ to alcohol formation [5,6]. Reduction of carbohydrates and carboxylic acids to alcohols during solventogenesis changes the requirements for reduced cofactors, increasing the demand for NADH and NADPH.

A bioinformatics based classification of *Clostridia* hydrogenases indicated *C. acetobutylicum* encodes a probable group 1 membrane associated [NiFe]-hydrogenase implicated in hydrogen uptake [9]. Increased transcript levels for the *C. acetobutylicum* [NiFe]-hydrogenase and maturation genes were observed during late solventogenesis in sessile cells, and evidence of H₂ uptake by the [NiFe]-hydrogenase in a related solventogenic organism indicated a solvent phase role for the *C. acetobutylicum* [NiFe]-hydrogenase [12,13]. *C. acetobutylicum* is unique because the hydrogenase genes and maturation factor genes are located on different genetic elements [9]: the chromosome and pSol megaplasmid, respectively (Figure 1). In the current study, the [NiFe]-maturation pathway was disrupted via interruption of *ca_c0810*, *hypF*, using the ClosTron type II intron system. A likely consequence of the *hypF* mutation was reduced HypD expression because the *hypD* gene is downstream of *hypF* in a polycistronic operon. Zymograms were used to show hydrogenase activity was similarly reduced in the $\Delta hypF/hypD$ mutant and M5 strain, providing evidence that chromosomally encoded HypF and HypD are important for the maturation of the megaplasmid encoded [NiFe]-hydrogenase. Furthermore, maturation of [FeFe]-hydrogenases requires a different set of maturation factors, so a disruption of [NiFe]-maturation was not expected to alter functional [FeFe]-hydrogenase production.

Acid and ABE formation were examined under several growth conditions to begin elucidating the [NiFe]-hydrogenase's metabolic role. The first condition comprised cultures subject to agitation in bioreactors, where the headspace was flushed with N₂. Under these growth conditions, levels of dissolved H₂ would be comparatively lower than other conditions examined, reducing impacts from potential loss of H₂ uptake in the $\Delta hypF/hypD$ mutant [6]. WT and the $\Delta hypF/hypD$ mutant in the first condition produced very little solvents and similar amounts of acetate and butyrate, indicating the [NiFe]-hydrogenase was not necessary for acidogenesis. The second condition examined planktonic cultures in bioreactors with zero agitation, where the headspace was flushed with N₂. This would lead to relatively higher dissolved H₂ levels as compared to agitated cultures. Under these conditions, the [NiFe]-hydrogenase appeared to be important for solvent production, since the $\Delta hypF/hypD$ mutant produced fewer solvents than the WT after 24 h, as shown in Table 1. A third condition, static planktonic growth in defined medium in an anaerobic chamber without N₂ headspace flushing, exacerbated this effect. In the static planktonic conditions the $\Delta hypF/hypD$ mutant produced higher butyrate and lower butanol levels when compared to WT, thereby indicating the mutant was defective in reduction of butyrate to butanol or was less tolerant to butanol accumulation. The reduced capacity to produce butanol could be due to low NADH and NADPH availability, as reduction of butyryl-CoA to butanol is thought to require one NADH and one NADPH [1]. The apparent lack of reduced cofactor availability in the $\Delta hypF/hypD$ mutant during static planktonic growth indicates that the [NiFe]-hydrogenase is important for reducing NAD⁺ and/or NADP⁺ via hydrogen uptake.

To further test if the [NiFe]-hydrogenase was important for solvent formation, metabolite output was examined under a fourth growth condition consisting of sessile cultures grown in a defined medium in an anaerobic chamber without N₂ headspace flushing. A recent study showed that growth in sessile conditions enhanced butanol production and that the [NiFe]-hydrogenase genes were induced during these conditions [41]. The $\Delta hypF/hypD$ mutant exhibited delayed growth, as indicated by the small changes in metabolite concentrations between 0 and 24 h shown in Figure 3. The $\Delta hypF/hypD$ mutant was ultimately able to recover, and during early solventogenesis the mutant had a higher acetone to butanol ratio than the WT, which is consistent with the inability to uptake H₂ for the reduction of butyryl-CoA to butanol. This is in agreement with a recent study showing a lack of reduced NAD(P)H availability increased acetone output in solvent phase [42]. Solventogenesis stalled

in the sessile $\Delta hypF/hypD$ mutant cultures between 48 h and 72 h, but resumed thereafter, presumably due to a shift in metabolism. During the solventogenic stall there was an increase in calculated net NADH formed from acid production when normalized to glucose consumption, suggesting there was compensation due to disruption of an NADH production pathway in the $\Delta hypF/hypD$ mutant. In the latter stages of solventogenesis of the sessile $\Delta hypF/hypD$ mutant cultures there was an increase in butanol, but not acetone or ethanol, and there was little to no net uptake of acetate and butyrate. This altered output/uptake profile suggests the $\Delta hypF/hypD$ mutant has a different electron flow for maintaining redox balance when compared to WT.

In order to determine the [NiFe]-hydrogenase's location, EFTEM Pd elemental mapping was used to identify locations of Pd(0) nanoparticles that were formed by *C. acetobutylicum* strains using H₂ gas as an electron donor. Pd(II) would be reduced to palladium(0) nanoparticles at the catalytic site of H₂ oxidation and thus identify the location of the hydrogenase [43]. Comparisons of the EFTEM mapping results between the strains indicated that the [NiFe]-hydrogenase is membrane localized with the catalytic subunit facing the extracellular side of membrane. This is evidenced by the decrease of Pd(0) nanoparticle deposits on the $\Delta hypF/hypD$ and M5 pSol megaplasmid null strain, when compared to wild type.

It was not possible to definitively determine the electron acceptor of the [NiFe]-hydrogenase based upon sequence analysis, but the putative heme binding protein encoded by *ca_p0144* is a strong candidate. A common mechanism for hydrogen uptake [NiFe]-hydrogenases is reduction of a cytochrome during H₂ oxidation [44]. The reduced cytochrome then serves as an electron shuttle to move electrons from the hydrogenase to other enzyme systems. The location of the [NiFe]-hydrogenase on the extracellular face of the membrane suggests that a mechanism likely exists for transfer of electrons to and intracellular enzyme system. Based upon previously measured cellular parameters, it was calculated that NAD⁺ reduction could be coupled to membrane transport of two electrons. The calculations were performed assuming 1 bar of H₂. Planktonic cultures can be supersaturated for H₂, resulting in an increase of reaction potentials, which could make some of the reactions, that were calculated to be slightly below zero, favorable [45].

Evidence presented above shows it is likely the [NiFe]-hydrogenase that allows for extracellular H₂ oxidation coupled to reduction of an intracellular electron acceptor. This activity, combined with the [FeFe]-hydrogenase activity, allows for hydrogen cycling, which could serve as a crude proton pump (see Figure 5B), similar to the mechanism of hydrogen cycling characterized in *Desulfovibrio* [38]. Butanol has been shown to disrupt the pmf of *C. acetobutylicum*, and the [NiFe]-hydrogenase could counter this disruption during solvent production [46]. In this scenario, the [NiFe]-hydrogenase could improve the efficiency of pmf maintenance through hydrogen cycling while providing the NADH needed for alcohol production. It is plausible that disruption of hydrogenase maturation, resulting in an inability to maintain pmf, was responsible for the initial stalling in solvent phase growth of the sessile $\Delta hypF/hypD$ mutant cultures.

During solventogenesis the [NiFe]-hydrogenase could generate the required NADH, but an NADPH source would still be required for butanol dehydrogenase. NADPH could be supplied by the ferredoxin:NAD(P) reductase. A recent report indicated augmented ferredoxin:NAD(P) reductase expression during the solvent phase increases relative butanol output, presumably by redirecting electron flow from H₂ production [41,47]. An alternative NADPH source could be NADP-dependent glyceraldehyde-3-phosphate dehydrogenase (GapN) [48]. A previous study showed that the *gapN* and [NiFe]-hydrogenase genes were induced during growth in sessile cultures, while genes for the glyceraldehyde-3-phosphate and phosphoglycerate kinase were repressed [12]. This suggests the route through glycolysis could be altered to compensate for increased NADPH demand. Calculations of reduction potentials using previously measured NAD⁺/NADH, NADP/NADP⁺, and internal pH values (see supplemental information) indicated the physiologic reduction potential is ~−260 mV for NAD⁺/NADH and ~−320 mV for NADP/NADP⁺. Due to this disparity, it is plausible that the cells have separate mechanisms to recycle the two cofactors.

This study demonstrates, to the best of our knowledge, the first evidence of hydrogen cycling as a potential energy conserving mechanism in *Clostridium. C. acetobutylicum* encodes for a group 4 [NiFe]-hydrogenase, not a group 1, that participates in hydrogen cycling to maintain the pmf for energy conservation and most likely produce NADH. The work highlights the need to improve knowledge of electron flow and membrane energetics in *C. acetobutylicum* in order to guide engineering strategies for directing product formation. Additionally, understanding how the $\Delta hypF/hypD$ mutant re-routed its metabolism during the latter phases of solventogenesis, when the major output was butanol, could lead to new strategies for the selective production of butanol.

Supplementary Materials: The following are available online at <http://www.mdpi.com/2311-5637/4/3/55/s1>

Author Contributions: K.L.G. performed zymograms, generated the $\Delta hypF/hypD$ mutant and complement strain, performed growth studies, performed palladium reduction studies, analyzed data, and wrote the manuscript. S.L. performed HPLC analysis of metabolites. E.S.G. performed growth studies, confirmed the $\Delta hypF/hypD$ mutant, performed palladium reduction studies, and edited the manuscript. R.L.R. performed RNAseq sample handling and analysis. M.D.S. performed experiments to establish knock out via southern blot and identify if there was nonspecific integration. T.N.K.Z. performed growth studies. H.D. performed sample embedding for TEM. A.M.S. performed microtome sample preparation and data collection for TEM and EFTEM. S.D.W. performed EFTEM mapping for palladium location. C.J.S. conceived of the project, analyzed data, and wrote the manuscript.

Funding: This research received no external funding.

Conflicts of Interest: The authors declare no conflict of interest.

References

1. Jones, D.T.; Woods, D.R. Acetone-butanol fermentation revisited. *Microbiol. Rev.* **1986**, *50*, 484–524. [PubMed]
2. Gapes, J.R. The economics of acetone-butanol fermentation: Theoretical and market considerations. *J. Mol. Microbiol. Biotechnol.* **2000**, *2*, 27–32. [PubMed]
3. Keis, S.; Shaheen, R.; Jones, D.T. Emended descriptions of *Clostridium acetobutylicum* and *Clostridium beijerinckii*, and descriptions of *Clostridium saccharoperbutylacetonicum* sp. nov. and *Clostridium saccharobutylicum* sp. nov. *Int. J. Syst. Evol. Microbiol.* **2001**, *51*, 2095–2103. [CrossRef] [PubMed]
4. Girbal, L.; Croux, C.; Vasconcelos, I.; Soucaille, P. Regulation of metabolic shifts in *Clostridium-acetobutylicum* ATCC-824. *FEMS Microbiol. Rev.* **1995**, *17*, 287–297. [CrossRef]
5. Cai, X.; Servinsky, M.; Kiel, J.; Sund, C.; Bennett, G.N. Analysis of redox responses during TNT transformation by *Clostridium acetobutylicum* ATCC 824 and mutants exhibiting altered metabolism. *Appl. Microbiol. Biotechnol.* **2013**, *97*, 4651–4663. [CrossRef] [PubMed]
6. Servinsky, M.D.; Liu, S.; Gerlach, E.S.; Germane, K.L.; Sund, C.J. Fermentation of oxidized hexose derivatives by *Clostridium acetobutylicum*. *Microb. Cell Fact.* **2014**, *13*, 139. [CrossRef] [PubMed]
7. Lutke-Eversloh, T.; Bahl, H. Metabolic engineering of *Clostridium acetobutylicum*: Recent advances to improve butanol production. *Curr. Opin. Biotechnol.* **2011**, *22*, 634–647. [CrossRef] [PubMed]
8. Girbal, L.; Vasconcelos, I.; Soucaille, P. Transmembrane pH of *Clostridium acetobutylicum* is inverted (more acidic inside) when the in vivo activity of hydrogenase is decreased. *J. Bacteriol.* **1994**, *176*, 6146–6147. [CrossRef] [PubMed]
9. Calusinska, M.; Happe, T.; Joris, B.; Wilmotte, A. The surprising diversity of clostridial hydrogenases: A comparative genomic perspective. *Microbiology* **2010**, *156*, 1575–1588. [CrossRef] [PubMed]
10. Demuez, M.; Cournac, L.; Guerrini, O.; Soucaille, P.; Girbal, L. Complete activity profile of *Clostridium acetobutylicum* [FeFe]-hydrogenase and kinetic parameters for endogenous redox partners. *FEMS Microbiol. Lett.* **2007**, *275*, 113–121. [CrossRef] [PubMed]
11. Yoo, M.; Bestel-Corre, G.; Croux, C.; Riviere, A.; Meynial-Salles, I.; Soucaille, P. A quantitative system-scale characterization of the metabolism of *Clostridium acetobutylicum*. *mBio* **2015**, *6*, e01808–e01815. [CrossRef] [PubMed]
12. Liu, D.; Xu, J.; Wang, Y.; Chen, Y.; Shen, X.; Niu, H.; Guo, T.; Ying, H. Comparative transcriptomic analysis of *Clostridium acetobutylicum* biofilm and planktonic cells. *J. Biotechnol.* **2016**, *218*, 1–12. [CrossRef] [PubMed]
13. Nakayama, S.; Kosaka, T.; Hirakawa, H.; Matsuura, K.; Yoshino, S.; Furukawa, K. Metabolic engineering for solvent productivity by downregulation of the hydrogenase gene cluster *hupCBA* in *Clostridium saccharoperbutylacetonicum* strain N1-4. *Appl. Microbiol. Biotechnol.* **2008**, *78*, 483–493. [CrossRef] [PubMed]

14. Clark, S.W.; Bennett, G.N.; Rudolph, F.B. Isolation and characterization of mutants of *Clostridium acetobutylicum* ATCC 824 deficient in acetoacetyl-coenzyme a: Acetate/butyrate: Coenzyme a-transferase (EC 2.8. 3.9) and in other solvent pathway enzymes. *Appl. Environ. Microbiol.* **1989**, *55*, 970–976. [[PubMed](#)]
15. Al-Shorgani, N.K.N.; Kalil, M.S.; Ali, E.; Yusoff, W.M.W.; Hamid, A.A. Enhancement of biobutanol production by butyric acid addition using *Clostridium saccharoperbutylacetonicum* N1-4 (ATCC 13564). *Biotechnology* **2012**, *11*, 326–332.
16. Servinsky, M.D.; Kiel, J.T.; Dupuy, N.F.; Sund, C.J. Transcriptional analysis of differential carbohydrate utilization by *Clostridium acetobutylicum*. *Microbiology* **2010**, *156*, 3478–3491. [[CrossRef](#)] [[PubMed](#)]
17. Heap, J.T.; Pennington, O.J.; Cartman, S.T.; Carter, G.P.; Minton, N.P. The clostron: A universal gene knock-out system for the genus clostridium. *J. Microbiol. Methods* **2007**, *70*, 452–464. [[CrossRef](#)] [[PubMed](#)]
18. Perutka, J.; Wang, W.; Goerlitz, D.; Lambowitz, A.M. Use of computer-designed group II introns to disrupt *Escherichia coli* DExH/D-box protein and DNA helicase genes. *J. Mol. Biol.* **2004**, *336*, 421–439. [[CrossRef](#)] [[PubMed](#)]
19. Heap, J.T.; Kuehne, S.A.; Ehsaan, M.; Cartman, S.T.; Cooksley, C.M.; Scott, J.C.; Minton, N.P. The clostron: Mutagenesis in clostridium refined and streamlined. *J. Microbiol. Methods* **2010**, *80*, 49–55. [[CrossRef](#)] [[PubMed](#)]
20. Servinsky, M.D.; Julin, D.A. Effect of a recD mutation on DNA damage resistance and transformation in *Deinococcus radiodurans*. *J. Bacteriol.* **2007**, *189*, 5101–5107. [[CrossRef](#)] [[PubMed](#)]
21. Tyurin, M.; Padda, R.; Huang, K.X.; Wardwell, S.; Caprette, D.; Bennett, G.N. Electrotransformation of *Clostridium acetobutylicum* ATCC 824 using high-voltage radio frequency modulated square pulses. *J. Appl. Microbiol.* **2000**, *88*, 220–227. [[CrossRef](#)] [[PubMed](#)]
22. Bolger, A.M.; Lohse, M.; Usadel, B. Trimmomatic: A flexible trimmer for illumina sequence data. *Bioinformatics* **2014**, *30*, 2114–2120. [[CrossRef](#)] [[PubMed](#)]
23. McClure, R.; Balasubramanian, D.; Sun, Y.; Bobrovskyy, M.; Sumbly, P.; Genco, C.A.; Vanderpool, C.K.; Tjaden, B. Computational analysis of bacterial RNA-Seq data. *Nucleic Acids Res.* **2013**, *41*, e140. [[CrossRef](#)] [[PubMed](#)]
24. Pinske, C.; Jaroschinsky, M.; Sargent, F.; Sawers, G. Zymographic differentiation of [NiFe]-hydrogenases 1, 2 and 3 of *Escherichia coli* K-12. *BMC Microbiol.* **2012**, *12*, 1. [[CrossRef](#)] [[PubMed](#)]
25. Finch, A.S.; Mackie, T.D.; Sund, C.J.; Sumner, J.J. Metabolite analysis of *Clostridium acetobutylicum*: Fermentation in a microbial fuel cell. *Bioresour. Technol.* **2011**, *102*, 312–315. [[CrossRef](#)] [[PubMed](#)]
26. Yong, P.; Rowson, N.A.; Farr, J.P.G.; Harris, I.R.; Macaskie, L.E. Bioreduction and biocrystallization of palladium by *Desulfovibrio desulfuricans* NCIMB 8307. *Biotechnol. Bioeng.* **2002**, *80*, 369–379. [[CrossRef](#)] [[PubMed](#)]
27. Huang, L.; Gibbins, L.N.; Forsberg, C.W. Transmembrane pH gradient and membrane potential in *Clostridium acetobutylicum* during growth under acetogenic and solventogenic conditions. *Appl. Environ. Microbiol.* **1985**, *50*, 1043–1047. [[PubMed](#)]
28. Amador-Noguez, D.; Feng, X.J.; Fan, J.; Roquet, N.; Rabitz, H.; Rabinowitz, J.D. Systems-level metabolic flux profiling elucidates a complete, bifurcated tricarboxylic acid cycle in *Clostridium acetobutylicum*. *J. Bacteriol.* **2010**, *192*, 4452–4461. [[CrossRef](#)] [[PubMed](#)]
29. Mao, F.L.; Dam, P.; Chou, J.; Olman, V.; Xu, Y. Door: A database for prokaryotic operons. *Nucleic Acids Res.* **2009**, *37*, D459–D463. [[CrossRef](#)] [[PubMed](#)]
30. Dam, P.; Olman, V.; Harris, K.; Su, Z.C.; Xu, Y. Operon prediction using both genome-specific and general genomic information. *Nucleic Acids Res.* **2007**, *35*, 288–298. [[CrossRef](#)] [[PubMed](#)]
31. Tjaden, B. *De novo* assembly of bacterial transcriptomes from RNA-Seq data. *Genome Biol.* **2015**, *16*, 1. [[CrossRef](#)] [[PubMed](#)]
32. Caspi, R.; Billington, R.; Ferrer, L.; Foerster, H.; Fulcher, C.A.; Keseler, I.M.; Kothari, A.; Krummenacker, M.; Latendresse, M.; Mueller, L.A.; et al. The metacyc database of metabolic pathways and enzymes and the biocyc collection of pathway/genome databases. *Nucleic Acids Res.* **2016**, *44*, D471–D480. [[CrossRef](#)] [[PubMed](#)]
33. Boratyn, G.M.; Schaffer, A.A.; Agarwala, R.; Altschul, S.F.; Lipman, D.J.; Madden, T.L. Domain enhanced lookup time accelerated BLAST. *Biol. Direct* **2012**, *7*, 12. [[CrossRef](#)] [[PubMed](#)]
34. Johnson, M.; Zaretskaya, I.; Raytselis, Y.; Merezuk, Y.; McGinnis, S.; Madden, T.L. NCBI BLAST: A better web interface. *Nucleic Acids Res.* **2008**, *36*, W5–W9. [[CrossRef](#)] [[PubMed](#)]

35. Muller, A.; MacCallum, R.M.; Sternberg, M.J.E. Benchmarking PSI-BLAST in genome annotation. *J. Mol. Biol.* **1999**, *293*, 1257–1271. [[CrossRef](#)] [[PubMed](#)]
36. Altschul, S.F.; Gish, W.; Miller, W.; Myers, E.W.; Lipman, D.J. Basic local alignment search tool. *J. Mol. Biol.* **1990**, *215*, 403–410. [[CrossRef](#)]
37. Paschos, A.; Bauer, A.; Zimmermann, A.; Zehelein, E.; Bock, A. Hypf, a carbamoyl phosphate-converting enzyme involved in [NiFe]-hydrogenase maturation. *J. Biol. Chem.* **2002**, *277*, 49945–49951. [[CrossRef](#)] [[PubMed](#)]
38. Odom, J.M.; Peck, H.D., Jr. Hydrogenase, electron-transfer proteins, and energy coupling in the sulfate-reducing bacteria *Desulfovibrio*. *Annu. Rev. Microbiol.* **1984**, *38*, 551–592. [[CrossRef](#)] [[PubMed](#)]
39. Wang, Y.; San, K.-Y.; Bennett, G.N. Cofactor engineering for advancing chemical biotechnology. *Curr. Opin. Biotechnol.* **2013**, *24*, 994–999. [[CrossRef](#)] [[PubMed](#)]
40. Vasconcelos, I.; Girbal, L.; Soucaille, P. Regulation of carbon and electron flow in *Clostridium-acetobutylicum* grown in chemostat culture at neutral pH on mixtures of glucose and glycerol. *J. Bacteriol.* **1994**, *176*, 1443–1450. [[CrossRef](#)] [[PubMed](#)]
41. Liu, D.; Chen, Y.; Li, A.; Ding, F.Y.; Zhou, T.; He, Y.; Li, B.B.; Niu, H.Q.; Lin, X.Q.; Xie, J.J.; et al. Enhanced butanol production by modulation of electron flow in *Clostridium acetobutylicum* B3 immobilized by surface adsorption. *Bioresour. Technol.* **2013**, *129*, 321–328. [[CrossRef](#)] [[PubMed](#)]
42. Liu, D.; Yang, Z.J.; Wang, P.; Niu, H.Q.; Zhuang, W.; Chen, Y.; Wu, J.L.; Zhu, C.J.; Ying, H.J.; Ouyang, P.K. Towards acetone-uncoupled biofuels production in solventogenic clostridium through reducing power conservation. *Metab. Eng.* **2018**, *47*, 102–112. [[CrossRef](#)] [[PubMed](#)]
43. Mikheenko, I.P.; Rousset, M.; Dementin, S.; Macaskie, L.E. Bioaccumulation of palladium by *Desulfovibrio fructosivorans* wild-type and hydrogenase-deficient strains. *Appl. Environ. Microbiol.* **2008**, *74*, 6144–6146. [[CrossRef](#)] [[PubMed](#)]
44. Frielingsdorf, S.; Schubert, T.; Pohlmann, A.; Lenz, O.; Friedrich, B. A trimeric supercomplex of the oxygen-tolerant membrane-bound [NIFE]-hydrogenase from *Ralstonia eutropha* H16. *Biochemistry* **2011**, *50*, 10836–10843. [[CrossRef](#)] [[PubMed](#)]
45. Paus, A.; Andre, G.; Perrier, M.; Guiot, S.R. Liquid-to-gas mass transfer in anaerobic processes: Inevitable transfer limitations of methane and hydrogen in the biomethanation process. *Appl. Environ. Microbiol.* **1990**, *56*, 1636–1644. [[PubMed](#)]
46. Terracciano, J.S.; Kashket, E.R. Intracellular conditions required for initiation of solvent production by *Clostridium acetobutylicum*. *Appl. Environ. Microbiol.* **1986**, *52*, 86–91. [[PubMed](#)]
47. Magnan, D.T.C.; San, K.Y.; Bennett, G.N. Modification of butyrate and butanol production in *Clostridium acetobutylicum* by introduction of a ferredoxin oxidoreductase. In Proceedings of the Rice University: SIMB Annual Meeting, New Orleans, LA, USA, 24–28 July 2016.
48. Iddar, A.; Valverde, F.; Serrano, A.; Soukri, A. Expression, purification, and characterization of recombinant nonphosphorylating NADP-dependent glyceraldehyde-3-phosphate dehydrogenase from *Clostridium acetobutylicum*. *Protein Expr. Purif.* **2002**, *25*, 519–526. [[CrossRef](#)]

